RBS 연결부를 갖는 보에 대한 부등 단면 보 요소

Non-Prismatic Beam Element for Beams with RBS Connection

김 기 동[1] · 고 만 기[2] · 황 병 국[3] · 배 창 규[4]
Kim, Kee Dong *Ko, Man Gi* *Hwang, Byoung Kuk* *Pae, Chang Kyu*

요 약 : 포스트-노스리지 연결부를 사용하는 강재 보의 탄성거동을 모델하기 위한 부등 단면 보 요소가 제안된다. 감소 단면 (RBS) 연결부를 갖는 부등단면 부재에 대한 탄성 강성 매트릭스는 수치적분이 필요치 않는 수식으로 표현되고 전단 효과를 포함하고 있다. 또한 균일 단면 보 요소를 사용하여 RBS 연결부를 갖는 보를 모델 하는 간략 방법이 제안된다. 이 방법의 장점은 기존의 보 요소를 사용하여 RBS 연결부를 사용하는 강재 모멘트 골조의 최대 층간 상대 변위 비를 상당히 정확하게 예측할 수 있다는데 있다. 강재 모멘트 골조의 탄성 강성에 감소 단면 연결부가 미치는 영향이 조사되었고, 절점에서의 변형을 고려하기 위한 적절한 모델 선정이 골조의 최대 층간 상대변위 비를 정확히 예측하는데 감소 단면 연결부보다 중요한 역할을 하였다.

ABSTRACT : This study presents a non-prismatic beam element for modeling the elastic behavior of steel beams, which have the post-Northridge connections in steel moment frames. The elastic stiffness matrix, including the shear effects for non-prismatic members with reduced beam section (RBS) connection, is in closed form. A simplified approach is also suggested, which uses a prismatic beam element to model beams with the RBS connection. This method can estimate quiteexactly the maximum story drift ratios of frames with the RBS connection. The effects of reduced beam section connection on the elastic stiffness of steel moment frames were investigated. The selection of a proper model to account for deformations at the joint might have a more important role in estimating the maximum story drift ratios of frames with better accuracy than the RBS cutouts.

핵 심 용 어 : 감소 단면 연결부, 부등 단면 보 요소, 강재 모멘트 골조, 층간 상대 변위 비, 포스트-노스리지 연결부
KEYWORDS : reduced beam section connection, non-prismatic beam element, steel moment frame, story drift ratio, post-Northridge conncection

1. General

The widespread damage to welded moment connections in moment-resisting frames (MRFs) during the 1994 Northridge earthquake undermined the confidence in the ductility of steel special MRFs. The most common failure mode was a brittle fracture in or around the complete joint penetration groove weld between the beam flanges and column flange (Youssef et al. 1995). Very little beam plastic deformation was observed in these connections. Since the Northridge earthquake, a great deal of research and testing has been conducted to identify better moment connections for new steel moment frame construction, as well as for repair or upgrading of existing steel moment frames. The majority of these efforts have combined improvements in welding together with modifications to the connection design. The modified connection design for special moment frames employs some type of reinforcement at the connection

1) 정회원, 공주대학교 토목환경공학과 교수, 공학박사
(Tel: 041-850-8631, Fax: 041-856-9388, E-mail: kkkim@kongju.ac.kr)
2) 정회원, 공주대학교 토목환경공학과 교수, 공학박사(mgko@kongju.ac.kr)
3) 정회원, 공주대학교 토목환경공학과 박사과정, 구조 기술사(hwangbyoungkuk@hotmail.com)
4) 정회원, 공주대학교 토목환경공학과 석사과정(paevision@yahoo.co.kr)

본 논문에 대한 토의를 2005년 6월 30일까지 학회로 보내주시면 토의 회답을 게재하겠습니다.

or radius-cut reduction of beam flanges near the column face in order to force the plastic hinge to occur away from the beam-column interface, as an accepted alteration of the pre-Northridge connection (FEMA 2000).

Reducing a beam section will decrease the stiffness of the beam and will, in turn, affect the elastic and inelastic behavior of the entire structure, influencing its internal loads and displacements. Although considerable researches and tests have been completed, some potentially important aspects of the modified connection have not been thoroughly investigated. One of these aspects is the effect of reduced beam sections (RBS) on the elastic stiffness of the frame and the other is on the dynamic nonlinear behavior of the frame. One research (Chambers, et. al 2003) indicated that about 11 % increase in elastic story drift was resulted from the standard reduction of 40 % flange width, while Grubbs (1997) showed that the elastic story drift due to the same flange reduction was increased by about 5 %. Most of researches (Chen, et. al 1996, Engelhardt, et. al 1996, Grubbs 1997, and Faggiano, et. al 2003) have suggested that the reduction in elastic stiffness due to RBS is likely to be small. Overall, however, very little research appears to have been done to accurately quantify the reduction in elastic stiffness of the frame due to RBS. Thus, the development of an analytical model for non-prismatic beams with the reduced beam section connection (RBS), which is fundamental to the quantification of both the elastic and inelastic performance of structures which incorporate the non-prismatic beams, and its application are the subject of this study.

2. General Description

The beam element presented in this paper (RBS beam element) is applicable to non prismatic members with the reduced beam section connection (RBS). The element will model the response of bare steel members subject to moment, axial force, and shear. It is intended to represent the clear span portion of beams in steel moment frames. Elastic shear deformations are included.

The element has two nodes. The nodes connect to the global structure and have three degrees of freedom each, namely translations and rotation in the local coordinate system, as shown in Figure 1. In the local coordinate system, if the rigid body motions are removed, the element can be considered as a simply supported beam. On the basis of equilibrium, all the components of local nodal forces R(R1 to R6) can be computed from the values of relative forces s(s1, s2, and s3). The transformation from the relative forces **s** to the nodal forces R is defined as

$$\mathbf{R} = \mathbf{A} \cdot \mathbf{s} \tag{1}$$

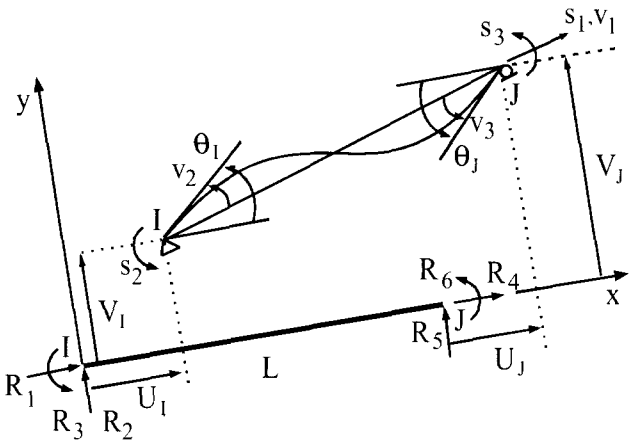

Fig 1. Element Relative Forces and Deformations in Local Coordinate System

where A is the force transformation matrix, which is well known and can be found in the literature (Przemieniecki 1968). From geometry, the transformation from the local displacements r to the relative deformations v(v1, v2, and v3) is accomplished by

$$\mathbf{v} = \mathbf{A}^{T} \cdot \mathbf{r} \tag{2a}$$

where $\mathbf{r}^{T} = \{U_i, V_i, \theta_i, U_j, V_j, \theta_j\}$ (2b)

3. Element Stiffness

The elastic element flexibility relationship is

determined by applying the Castigliano's theorem to the non-prismatic element shown in Figure 2, as follows:

$$\mathbf{dv} = \mathbf{f_e} \cdot \mathbf{ds} \tag{3a}$$

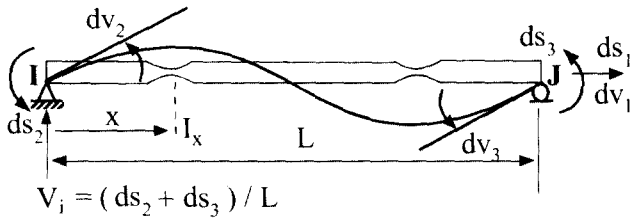

Fig 2. Non-prismatic Beam Element.

where ds(ds1, ds2, and ds3)is the action increment and fe is the elastic flexibility matrix which includes the effects of shear, in which

$$\mathbf{f_e} = \begin{bmatrix} \int_0^L \frac{1}{EA_x}dx & 0 & 0 \\ 0 & \int_0^L \frac{(\xi-1)^2}{EI_x}dx + \int_0^L \frac{1}{L^2GA_x^s}dx & \int_0^L \frac{(\xi-1)\xi}{EI_x}dx + \int_0^L \frac{1}{L^2GA_x^s}dx \\ 0 & \int_0^L \frac{(\xi-1)\xi}{EI_x}dx + \int_0^L \frac{1}{L^2GA_x^s}dx & \int_0^L \frac{\xi^2}{EI_x}dx + \int_0^L \frac{1}{L^2GA_x^s}dx \end{bmatrix} \tag{3b}$$

where EA_x, GA_x^s and EI_x are axial, effective shear, and flexural rigidity at the arbitrary distance x, respectively, and ξ is x/L. By integrating each element in the flexibility matrix for a beam with RBS shown in Figure 3, the elastic flexibility matrix fe is converted as follows:

$$\mathbf{f_e} = \begin{bmatrix} \frac{L}{EA} f_a & 0 & 0 \\ 0 & \frac{L}{EI} f_{ii} + \frac{1}{LGA} f_s & \frac{L}{EI} f_{ij} + \frac{1}{LGA} f_s \\ 0 & \frac{L}{EI} f_{ij} + \frac{1}{LGA} f_s & \frac{L}{EI} f_{ij} + \frac{1}{LGA} f_s \end{bmatrix} \tag{4}$$

where A= gross area of the cross section; I=gross moment of inertia of the cross section; L=beam length.

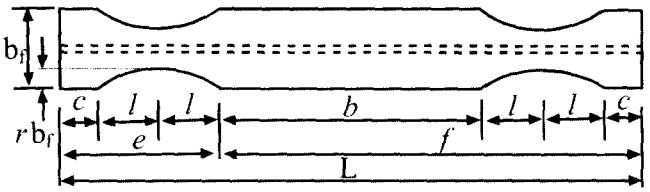

Fig 3. Non-prismatic Beam with Reduced Beam Sections.

The integration procedure can be found in the literature (Chambers 2003). The flexibility coefficients f_{ii} and f_{ij} related to the flexure can be expressed as

$$f_{ii} = f_{jj} = \frac{l}{3L^3}\left[2c^3 + 3Lc(L-c) + (L-c-2l)^3 - (c+2l)^3\right] + \frac{l}{L^3 4n}\left\{2\Lambda - 2\gamma\left(e^2 + f^2 + 2R^2\right) + \left[e^2 + f^2 + 2R^2\left(1 - \frac{1}{\alpha^2}\right)\right]\cdot\Psi\right\} \tag{5a}$$

$$f_{ij} = f_{ji} = -\frac{l}{6L^3}\left[L^3 - 24L(c+l)l + 8l\left(3c^2 + 6cl + 4l^2\right)\right] + \frac{l}{L^3 2n}\left\{\Lambda - 2\gamma\left(R^2 - ef\right) - \left[ef - R^2\left(1 - \frac{1}{\alpha^2}\right)\right]\cdot\Psi\right\} \tag{5b}$$

$$\Lambda = R^2\left\{\gamma + \frac{1}{2}\sin 2\gamma + \frac{2}{\alpha}\left(\sin\gamma + \frac{\gamma}{\alpha}\right)\right\},$$
$$\Psi = \frac{4}{\sqrt{1-\alpha^2}}\tan^{-1}\left(\sqrt{\frac{1+\alpha}{1-\alpha}}\tan\frac{\gamma}{2}\right) \tag{5c}$$

where $\alpha = \mu/\beta$; $\beta = 1 - 4na$; $\gamma = \sin^{-1}(l/R)$; $\mu = 4Rn$; $R = (r^2 b_f^2 + l^2)/(2rb_f)$; $a = rb_f - R$; $n = 1/I\{t_f^3/12 + [(d-t_f)/2]^2 t_f\}$, the radius of flange reduction; b_f = beam flange width; t_f = beam flange thickness; and d = beam depth. The flexibility coefficient f_a related to the axial deformation is defined as

$$f_a = \frac{(b+2c)}{L} + \frac{4}{Ln_a}\left\{-\gamma + \frac{2}{\sqrt{1-\alpha_a^2}}\tan^{-1}\left(\sqrt{\frac{1+\alpha_a}{1-\alpha_a}}\tan\frac{\gamma}{2}\right)\right\} \tag{5d}$$

where $n_a = 4t_f/A$; $\beta_a = 1 - n_a a$; $\mu_a = R\, n_a$; and

$\alpha_a = \mu_a / \beta_a$. The form factor for shear of a member with RBS, f_s is define as

$$f_s = \frac{A}{L}\int_0^L \frac{\chi_x}{A_x} dx \tag{5e}$$

where $A_x = A[1 - n_a\{\sqrt{(R^2 - x^2)} + a\}]$, the area of cross section at the arbitrary distance x; χ_x = form factor for shear of the cross section at the arbitrary distance x. The form factor χ_x at the distance x is defined as

$$\begin{aligned}\chi_x &= \int_A \frac{Q_x^2 A_x}{I_x^2 b_x^2} dA \\ &= \frac{9}{2}\left[\frac{1}{p_x}(1-t)+t\right] \cdot \\ &\quad \frac{\left[\frac{1}{p_x^2}\left(\frac{t^5}{2} - t^3 + \frac{t}{2}\right)\right]}{\left[\frac{1}{p_x}(1-t^3)+t^3\right]^2} + \\ &\quad \frac{\left[\frac{1}{p_x}\left(-\frac{23t^5}{30} + t^3 - \frac{t}{2} + \frac{8}{30}\right) + \frac{8t^5}{30}\right]}{\left[\frac{1}{p_x}(1-t^3)+t^3\right]^2}\end{aligned} \tag{5f}$$

where Q_x = first moment of the cross sectional area above the point where the shear stress is desired; I_x = moment of inertia of the cross section; b_x = breadth of the cross section at the point where the shear stress is desired; $t = (d/2 - t_f)/(d/2)$; $p_x = t_w/[b_f - 2(\sqrt{R^2 - x^2} + a)]$; t_w = beam web thickness. It is noted that for prismatic members the form factor f_s is equal to the form factor χ_x ($\cong A/(d \cdot t_w)$) of a cross section. Having determined the 3x3 flexibility matrix $\mathbf{f_e}$, this matrix is inverted to obtain a 3x3 stiffness matrix $\mathbf{k_e}$.

$$\mathbf{k_e} = \begin{bmatrix} \frac{EA}{L}k_a & 0 & 0 \\ 0 & \frac{EI}{L}\frac{s_{ii}}{s_{ii}^2 - s_{ij}^2} & -\frac{EI}{L}\frac{s_{ij}}{s_{ii}^2 - s_{ij}^2} \\ 0 & -\frac{EI}{L}\frac{s_{ij}}{s_{ii}^2 - s_{ij}^2} & \frac{EI}{L}\frac{s_{ii}}{s_{ii}^2 - s_{ij}^2} \end{bmatrix} = \begin{bmatrix} \frac{EA}{L}k_a & 0 & 0 \\ 0 & \frac{EI}{L}k_{ii} & \frac{EI}{L}k_{ij} \\ 0 & \frac{EI}{L}k_{ji} & \frac{EI}{L}k_{jj} \end{bmatrix} \tag{6}$$

where $k_a = 1/f_a$, $s_{ii} = f_{ii} + f_s EI/(L^2 GA)$, and $s_{ij} = f_{ij} + f_s EI/(L^2 GA)$.

4. Comparison to Finite Element Analysis

The tip displacements of various cantilever beams obtained by the RBS beam element were compared to the average nodal displacements obtained by finite-element analysis (FEA). The three following structural steel shapes were used in the analyses: W36X150, W30X148, and W24X68. Twelve different cantilever beams were analyzed. The three different size beams were each modeled for two cases: with and without the reduced beam section connection. Each case was then modeled for two different beam lengths of 15 feet (4.57m) and 20 feet (6.10m). The modeled cross sections differ slightly from the standard rolled structural shapes in the fact that those have sharp corners instead of filleted corners between the flanges and web. The dimensions of the cutouts (RBS) applied to various beam sizes modeled are shown in Table 1.

Table 1. Dimensions of Reduced Beam Sections

Cross Section	c in. (cm)	$2l$ in. (cm)	$r \cdot b_f$ in. (cm)
W36x150	9 (22.86)	27 (68.58)	2.375 (6.03)
W30x148	5 (12.70)	25 (63.50)	2.0 (5.08)
W24x68	5 (12.70)	16 (40.64)	1.75 (4.45)

In each case, approximately 40 percent of beam flange width (r=0.2) was removed at the minimum section of the cutouts. In the finite element analysis the beam was discretized into 3600-4080 eight node hexahedron brick elements for 15 feet beam length and 4800-5440 brick elements for 20 feet beam length to get as much accurate results as possible. Linear elastic analyses were conducted with the finite element software ABAQUS (1996). The modulus of elasticity was equal to 29,000 ksi (199.9 GPa), and Poison's ratio was equal to 0.3. A concentrated load was placed

at the tip. This applied tip load was equally distributed to the beam web element nodes. The tip displacement obtained from FEA was the average value of the tip displacements at web element nodes. The results are presented in Table 2.

Table 2. Comparison of Tip Displacements Obtained by RBS Beam Element and FEA

Model	Tip Displacement (cm)						
	Prismatic Beam			Beam with RBS			Stiffness Decrease (%)
	Closed Form	FEA	Difference (%)	RBS Element	FEA	Difference (%)	
W36x150							
15′ Span	5.46	5.47	0.09	5.93	5.95	0.27	8.07
20′ Span	12.44	12.42	0.11	13.33	13.36	0.20	6.99
W30x148							
15′ Span	7.25	7.25	0.10	7.88	7.89	0.11	8.09
20′ Span	16.61	16.62	0.06	17.80	17.81	0.07	6.71
W24x68							
15′ Span	25.67	25.68	0.03	27.21	27.30	0.33	5.94
20′ Span	59.70	59.71	0.02	62.55	62.71	0.26	4.78

In order to evaluate the accuracy of the finite element model, the tip displacements predicted by the finite element analysis for prismatic cantilever beams were compared to a simplified closed form solution. The closed form tip displacement was computed as follows:

$$\Delta = \frac{Pl_b^3}{3EI} + f_s \frac{Pl_b}{AG} \tag{7}$$

where $f_s = A/A_w = A/(d \cdot t_w)$, the form factor for shear of a prismatic member; l_b = length of cantilever beam; P=tip load. The difference between the two solutions is small, typically less than 0.11 percent. The close agreement between these solutions suggests that the finite element analysis is providing accurate estimates of displacements. In order to evaluate the accuracy of the RBS beam element, the tip displacements predicted by the RBS beam element for cantilever beams with RBS were compared to the results of the finite element analysis (FEA). By considering equivalent cantilever beams of an anti-symmetric beam with RBS as shown in Figure 4, the tip displacement predicted by the RBS beam element can be computed as follows:

$$\Delta = \frac{2Pl_b^3}{(k_{ii} + k_{ij})EI} \tag{8}$$

where k_{ii} and k_{ij} are the stiffness coefficients obtained from Eq. 6 for an anti-symmetric beam with beam length of $2l_b$ as shown in Figure 4.

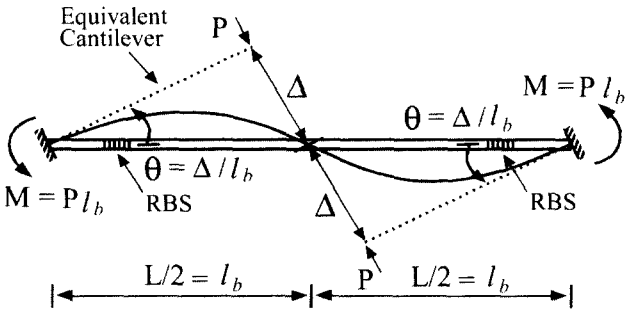

Fig 4. Equivalent Cantilever Beams.

It is noted that for prismatic members Equation 8 is reduced to Eq. 7. The difference between the tip displacements obtained by the RBS beam element and FEA is small, typically less than 0.33 percent. The close correlation between these results suggests that the RBS beam element is providing accurate estimates of displacements. By comparing the tip displacements of a beam with and without RBS, the percent reduction in stiffness of the beam due to RBS was calculated. The RBS connection with the flange reduction of 40 % (r=0.2) resulted in a reduction in stiffness of about 5-8 percent for the cantilever beams. The larger beams, W36X150 and W30X148, displaced a slightly higher reduction in stiffness than the smaller W24X48 beam. The longer spans tended to show a lower reduction in stiffness than the shorter spans. The reduction in overall frame stiffness due to RBS in the beams will be investigated later using the RBS beam element.

5. Parametric Study

A change of the reduction in stiffness coefficients due to variation of the cut dimensions is presented in

Figure 5. A W36x150 beam is modeled to have reduced beam sections as shown in Figure 3. The dimensions of a typical reduced beam section were suggested by FEMA 350 (FEMA 2000). The distance "c", which is measured from the face of the column to the start of RBS, was suggested in the range of $0.5b_f$ to $0.75b_f$, and the length of the cut, "$2l$", was suggested to be approximately 65 to 85 percent of the beam depth. The values of the flange reduction factor "r", which is the ratio of maximum depth of cut to flange width, were suggested in the range of 0.2 to 0.25. Using the limit values of the recommended ranges for the cut dimensions, the effects of variation of the cut dimensions on the reduction in stiffness coefficients are investigated.

Figure 5(a) presents the results of changes in the ratio of the distance "c" to flange width b_f. The beam length of 30 feet (9.1m=10d) was used. As the distance "c" increases, the reduction in k_{ii} and k_{ij} decreases. The location of the cut has no effect on the axial stiffness coefficient k_a. Three different dimensions of the cut were used as follows: 1) l/d =0.325 and r=0.2; 2) l/d=0.425 and r=0.2; 3) l/d =0.325 and r=0.25. From the comparison of the results for the three different dimensions of the cut, it can be seen that the increase of 25 percent in the flange reduction factor "r" has larger effects on the reduction in k_{ii} and k_{ij} than the increase of 30 percent in the cut length "$2l$".

Figure 5(b) presents the results of changes in the ratio of the half of the cut length "l" to beam depth d. As the cut length "$2l$" increases, the reduction in stiffness coefficients k_{ii}, k_{ij}, and k_a increases. Three different pairs of parameters "r" and "L" were used as follows: 1) r=0.2 and L/d=15; 2) r=0.25 and L/d=15; 3) r=0.2 and L/d=10. From the comparison of the results for the three different pairs of the parameters, it can be seen that for the suggested range on "l" of 0.325d to 0.425d, the increase of 25 percent in the flange reduction factor "r" has the similar effects on the reduction in k_{ii} and k_{ij} as the decrease of 33 percent in the beam length "L".

Figure 5(c) presents the results of changes in the flange reduction factor "r". The beam length of 30 feet was used. As the flange reduction factor "r" increases, the reduction in stiffness coefficients k_{ii}, k_{ij}, and k_a increases. Three different pairs of parameters "c" and "l" were used as follows: 1) c/b_f =0.75 and l/d =0.425; 2) c/b_f=0.75 and l/d=0.325; 3) c/b_f=0.5 and l/d=0.325. From the comparison of the results for the three different pairs of the parameters, it can be seen that the increase of 30 percent in the cut length "$2l$" has much larger effects on the reduction in k_{ii} and k_{ij}than the decrease of 33 percent in the distance "c".

Figure 5(d) presents the results of changes in the ratio of the beam length L to its depth d. As the beam length L increases, the reduction in stiffness coefficients k_{ii}, k_{ij}, and k_a decreases. Two different dimensions of the cut were used as follows: 1) c/b_f =0.5, l/d=0.425, and r=0.25; 2) c/b_f =0.75, l/d =0.325, and r=0.2. The first dimension provides the largest reduction in stiffness among the various cut dimensions satisfying the recommended ranges of parameters, and the second one gives the smallest reduction in stiffness. From the comparison of the results for the two different dimensions of the cut, it can be seen that the first dimension provides 8.7, 5.4, and 1.5 % larger reduction in k_{ii}, k_{ij},, and k_a, respectively, for the beam length of L=30 feet than the second one.

In general, the beam flange reduction factor "r" has the largest effects on the reduction in stiffness, and the beam length is the second to the largest.

As the beam flange reduction or the cut length increases, the reduction in stiffness increases. As the beam length or the parameter "c" increases, the reduction in stiffness decreases. The parameter "c" has negligible effects on the reduction in stiffness.

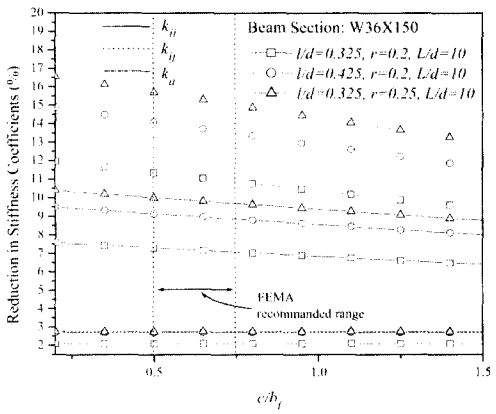

(a) Effect of the Ratio of Cut Location to Beam Depth

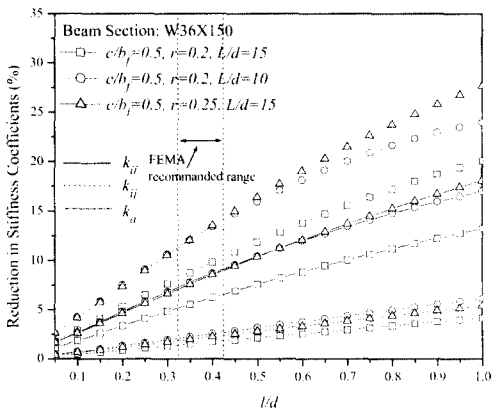

(b) Effect of the Ratio of Cut Length to Beam Depth

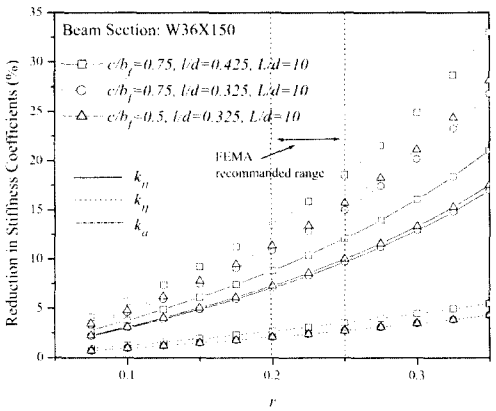

(c) Effect of the Ratio of Maximum Depth of Cut to Flange Width

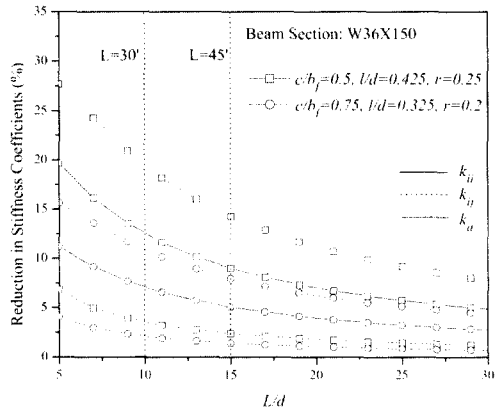

(d) Effect of the Ratio of Beam Length to Beam Depth

Fig 5. Effect of Cut Dimensions on the Reduction in Stiffness Coefficients.

The effect of the cuts on the reduction in lateral stiffness of one story-one bay frames is presented in Figure 6. The results were obtained by using center to center line dimensions of the frames. The lateral stiffness k_l of the frames is defined as the ratio of lateral roof load to lateral roof displacement as shown in the inlet of Figure 6 Various W-shape sections, which are efficient in beam applications, are applied to beams of the frames to investigate the effect of the cuts on the reduction in stiffness of various size beams. The values of $c/b_f=0.5$, $l/d=0.425$, and $r=0.25$ for the dimensions of the cuts were selected to produce the possible largest reduction in the lateral stiffness that a set of values within the recommended ranges of the cut dimensions produce. The typical beam length of $L=30$ feet was applied to the frames. The dimensions of columns were determined from the ratio of beam flexural stiffness to column flexural stiffness that made the reduction in lateral stiffness of the frame due to the cuts the largest as compared to the lateral stiffness of the corresponding frames without the cuts. The same size of cross section and the same length were applied to all columns. From Figure 6, it can be seen that as the weight per unit

length of W sections increases for the same beam depth or the depth of W sections increases for the same weight per unit length, the reduction in lateral stiffness increases. In general, the greater the depth and the weight per unit length, the larger the reduction in lateral stiffness.

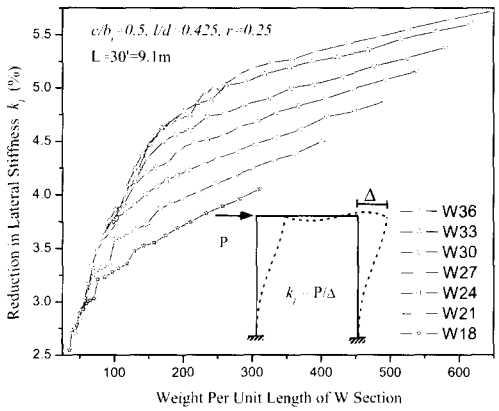

Fig 6. Reduction in Lateral Stiffness of One Story-One Bay Frame Due to RBS

To investigate the effect of the cuts on the form factor for shear f_s, the difference between the form factors for W36X150 beams with and without RBS is presented in Figure 7. Also shown in this figure are the differences between stiffnesses obtained by applying the above two different form factors to W36X150 beams with RBS. The values of parameters for the dimensions of the cuts were the same as those used above. For the beam length of L=30 feet, the difference between the form factors is 0.18 %, and the differences for k_{ij}, k_{ii}, , and k_l are 0.02 % , 0.01 % , and 0.002 % , respectively. As the beam length increases, these differences decrease. The difference between the form factors is very small, and the differences for the stiffnesses are much smaller. Practically, the form factor for a prismatic beam can be applied to the corresponding size beam with RBS with negligible error.

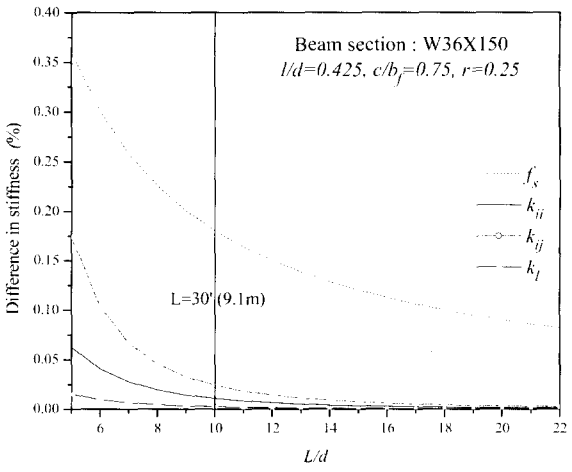

Fig 7. Effect of the Cuts on Form Factor for Shear

The effect of the cuts on the reduction in lateral stiffness of eight different frames is presented in Figure 8. The number of stories and bays was varied to investigate the effect of the cuts on the reduction in lateral stiffness of various size frames. The values of parameters for the dimensions of the cuts were the same as those used above. The dimensions of columns were determined from the ratio of beam flexural stiffness to column flexural stiffness that made the reduction in lateral stiffness the largest as for the above case. The same size of cross section was applied to all beams of each frame. The two different structural steel shapes W36X150 and W24X68 were used for beams. For all columns of each frame, the same size of cross section and the same length were also used. From Figure 8, it can be seen that the reduction in lateral stiffness is not much changed regardless of the number of bays. As the number of stories increases, the reduction in lateral stiffness increases at a decreasing rate. For the same length of beams, W36X150 beams produce larger reduction in lateral stiffness than W24X68 beams as for the previous case, and the difference between the results for the two different size beams increases as the number of stories increases.

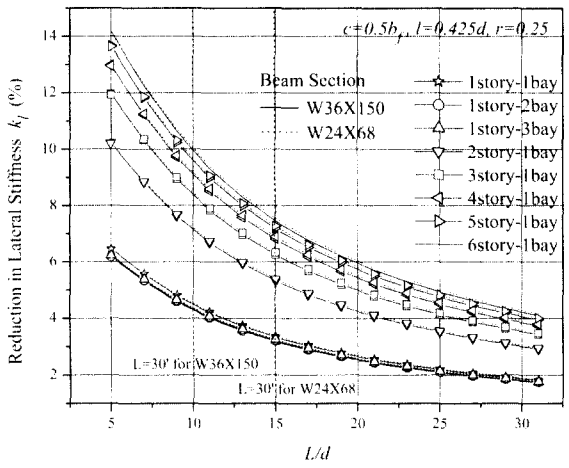

Fig 8. Reduction in Lateral Stiffness of Various Frames Due to RBS

6. Simplified Approach

While the finite element approach can provide accurate results, its usefulness for analyzing entire frames is limited due to the computational efficiency, and the extensive effort required in developing the model. Further, this approach does not lend itself well to routine design office use. If it is allowed to input stiffness coefficients k_{ii}, k_{jj}, and k_{ij} in commercial structural analysis computer programs, the developed element can be easily implemented in them. However, it is not usual for the computer programs. Consequently, a simplified approach will be developed for evaluating the change in elastic stiffness resulting from reduced beam sections in the beams of moment frames subjected to lateral loads.

In typical design practice, beams and columns are analyzed using one-dimensional frame elements. The simplified approach will be to model beams with the RBS connection by employing a prismatic beam element. In order to model beams with the RBS using a prismatic beam element, the properties of the element must be modified to reflect the changes in cross section. In this approach, an effective moment of inertia I_e is determined from equating the moment rotation relation of the idealized beam (Figure 9b) to that of the real beam with reduced beam sections (Figure 9a) while assuming the distribution of earthquake induced moments as an anti-symmetric condition. The effective moment of inertia I_e can be obtained as follows:

$$I_e = \frac{k_{ii} + k_{ij}}{6} I \tag{9}$$

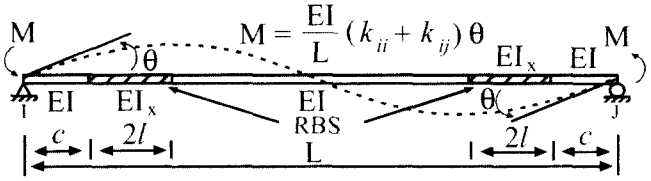

(a) Real Beam with Reduced Beam Sections

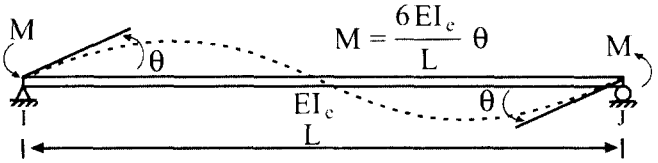

(b) Idealized Beam with Effective Moment of Inertia

Fig 9. Idealization of Beams with Reduced Beam Sections.

The procedure of the simplified approach is as follows; 1) for given beam dimensions and RBS dimensions, the stiffness coefficients k_{ii} and k_{ij} are determined from Eqs. 5 and 6; 2) using the resulting stiffness coefficients k_{ii} and k_{ij} an effective moment of inertia I_e for the idealized beam can be determined from Eq. 9.

A change of the effective moment of inertia due to variation of RBS dimensions is presented in Figure 10. The structural steel shape W36X150 was used for beams. From this figure it can be seen that the flange reduction factor "r" and the beam length "L" have larger effects on the change of the effective moment of inertia than the cut length "$2l$" and the distance "c" as in the parametric study. As the beam flange reduction or the cut length increases, the effective moment of inertia I_e decreases. As the beam length "L" or the parameter "c" decreases, the effective moment of inertia I_e decreases. The

parameter "c" has negligible effects on the change of the effective moment of inertia. In general, the effective moment of inertia I_e is influenced most by the beam flange reduction factor "r" and the beam length L.

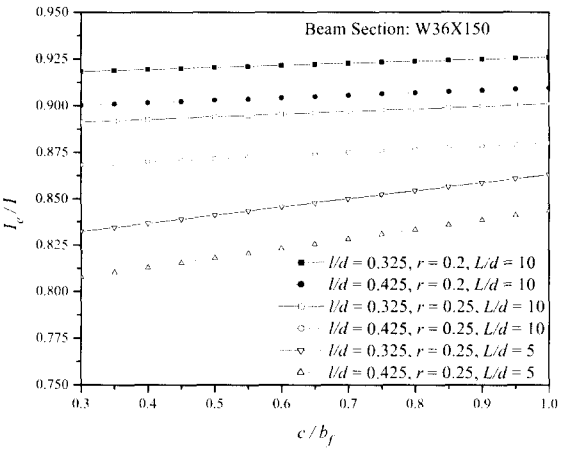

Fig 10. Change of Effective Moment of Inertia Due to Variation of Cut Dimensions

The effective moment of inertias of idealized beams are presented in Figures 11 and 12 for various W-shape sections, which are efficient in beam applications. The beam flange reduction of

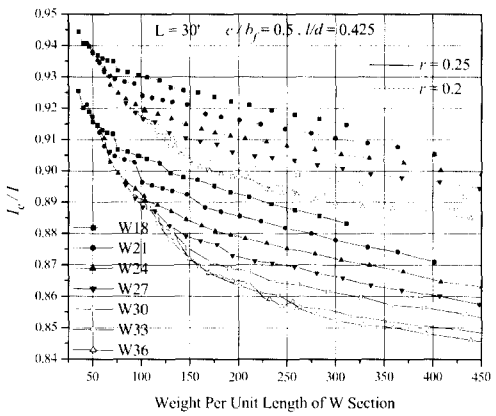

Fig 11. Effective Moment of Inertia of Various Beam Sections for Beam Length of L=30

40 % and 50 % is applied to obtain these figures. The values of c/b_f=0.5 and l/d =0.425 were selected to produce the smallest effective moment of inertia that a pair of values within the recommended results for the typical beam length of 30 feet are shown in Figure 11 and for the beam length of 20 feet in Figure 12. From Figure 11, it can be seen that as the weight per unit length of W sections increases or the depth of W sections increases, the effective moment of inertia decreases with little fluctuation. The effective moment of inertia for the flange reduction of 50 % (r=0.25) is about 2 to 5 % smaller than that for the flange reduction of 40 % (r=0.2) as the weight per unit length increases. The values of effective moment of inertia for the flange reduction 40 % and 50 % are within the range of 0.885I to 0.944I and 0.845I to 0.926I, respectively. From Figure 12, it can be seen that the values of effective moment of inertia for the beam length of 20 feet are within the range of 0.858I to 0.923I for the flange reduction 40 % and 0.811I to 0.898I for the flange reduction 50 %. Since the effective moment of inertias of various W-beam sections for a given flange reduction are within the narrow range, the effective moment of inertia of I_e=0.86I for the flange reduction of 40 % or I_e=0.81I for the flange reduction of 50 % will produce the conservative results with some error for various W-beam sections with the beam

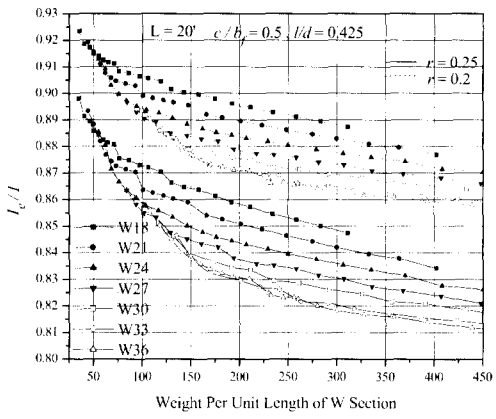

Fig 12. Effective Moment of Inertia of Various Beam Sections for Beam Length of L=20'

length of 20 feet, and for various W-beam sections with the beam length of 30 feet the effective moment of inertia of I_e=0.88I for the flange

reduction of 40 % However, it is suggested that the exact effective moment of inertia should be applied to the simplified approach because the simplified approach has some inherent error and the exact one can be easily obtained from Eq. 9 or Figures 11 and 12 with little effort.

7. Frame Analysis

In order to examine the effects of the RBS cutouts on lateral frame stiffness for a wide range of conditions, static analyses were conducted for three different steel moment frames: three-story four-bay, nine-story five-bay, and twenty-story five-bay frames. The design of the frames was to conform to the provisions of UBC 1994 (ICBO 1994) and FEMA 267(FEMA 1995). Details and dimensions of the frames are shown in Figure 13 and further information can also be found in the literature (Gupta and Krawinkler 1999). The lateral loading is distributed triangularly along the story height as shown in Figure 13. Since the change in stiffness caused by the RBS cutouts is of interest in this study, the total magnitude of the lateral loading is irrelevant. The three different frames were each modeled for two cases: with and without the RBS cutouts. The beam flange reductions of 40 % and 50 % were applied to frames with the RBS cutouts. The values of c/b_f = 0.5 and l/d = 0.425 were used for the beams with the RBS cutouts. The beams with the RBS cutouts were modeled by both the RBS beam element and the simplified approach. The following three different models were then applied to each case to describe the behavior of the beam-to-column joint region. The first model (CTC) is based on center-to-center line dimensions of frames. The second one (REO) uses 50 percent rigid end offsets, which models 50 percent of the actual joint dimension as rigid links to account approximately for deformations within the joint region. The last model (PZ) employs a panel zone

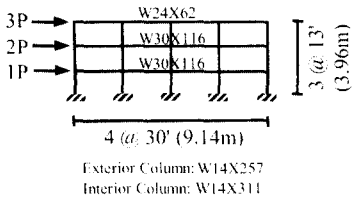

(a) 3 story- 4 bay frame

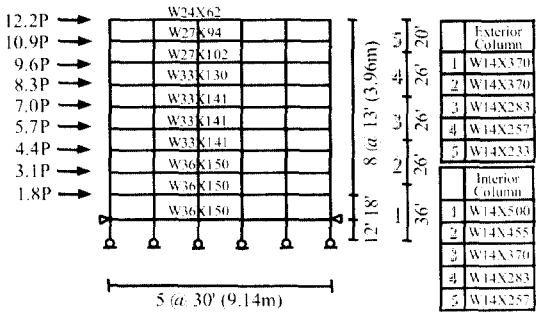

(b) 9 story- 5 bay frame

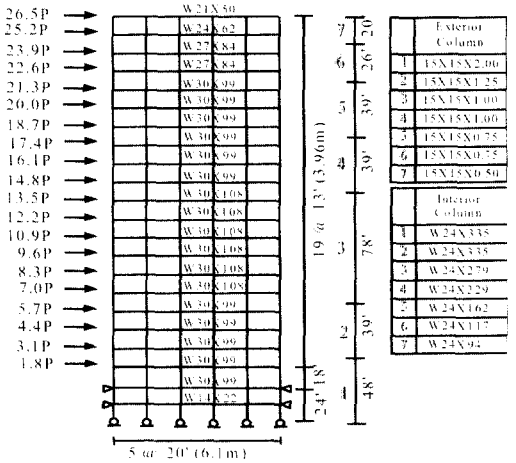

(c) 20 story- 5 bay frame

Fig 13. Model Frames

element with the rotational elastic stiffness equal to $G \cdot d_c \cdot t_{cw} \cdot d/(l-d/h)$ to describe the behavior of the joint, in which d_c = column depth; t_{cw} = column web thickness; d = beam depth; h = column height. The total forty five frame models were analyzed.

The percent increases in the maximum story drift and the roof displacement for 3-story, 9-story, and 20-story frames are presented in Table 3. The maximum story drift ratio is the maximum value

among the story drift ratios of each story for a particular frame. For the same size cutout, there appears to be few, if any, consistent trends in how the variation of the reduction in lateral stiffness is related to the type of frames. When 50 percent of the flange width is cutout, the increase in maximum story drift ranges from 6.7 to 7.5 percent, from 7.1 to 7.9 percent, and from 6.2 to 8.1 percent for CTC, REO, and PZ models, respectively. For the cutout of 40 percent, the increase in maximum story drift is 4.9 to 5.5 percent, 5.2 to 5.7 percent, and 4.5 to 5.9 percent for CTC, REO, and PZ models, respectively. As far as the increase in the roof displacement is concerned, the increase for the cutout of 50 % is 7 to 9 percent, 7.5 to 9 percent, models, respectively. For the cutout of 40 percent, and 6.1 to 7.3 percent for CTC, REO, and PZ the increase in the roof displacement is 5.2 to 6.6 percent, 5.5 to 6.6 percent, and 4.3 to 5.3 percent for CTC, REO, and PZ models, respectively. In general, the REO model produces the largest reduction in the lateral stiffness of frames and the PZ model provides the smallest one.

In Table 4, the maximum story drift ratios and the roof displacements, which are normalized to the result of CTC model for frames without RBS, are shown. From this table, it can be seen that the results of CTC model for frames without RBS cutouts are much larger for all frame types than those of REO model for frames with the flange reduction of 50 %, and are larger for high story frames than those of PZ model for frames with the flange reduction of 50 %. The results of PZ model for frames with the 40 percent flange reduction are larger than those of REO model for frames with the flange reduction of 50 %. From this fact, it should be noted that the selection of proper model to account for deformations at the joint might havethan the RBS cutouts.

larger influence on the lateral stiffness of frames

Figure 14. shows the comparison of maximum story drift ratios obtained by both the RBS beam element and the simplified approach. From this figure and Table 3, it can be seen that there is

Table 3. Increases in Maximum Story Drift and Roof Displacement

Frame	Increase in Maximum Story Drift (%)					
	RBS Element			Simplified Approach		
Model	CTC	REO	PZ	CTC	REO	PZ
3 story						
50% cut	7.32	7.86	6.22	7.32	7.87	6.23
40% cut	5.35	5.74	4.54	5.35	5.75	4.56
9 story						
50% cut	6.69	7.14	6.36	6.70	7.15	6.37
40% cut	4.88	5.21	4.64	4.89	5.21	4.65
20 story						
50% cut	7.47	7.50	8.11	7.48	7.51	8.11
40% cut	5.50	5.52	5.93	5.50	5.52	5.93
Frame	Increase in Roof Displacement (%)					
	RBS Element			Simplified Approach		
Model	CTC	REO	PZ	CTC	REO	PZ
3 story						
50% cut	7.06	7.49	6.06	7.07	7.49	6.07
40% cut	5.16	5.47	4.43	5.17	5.47	4.43
9 story						
50% cut	8.13	8.68	7.29	8.14	8.68	7.29
40% cut	5.92	6.32	5.30	5.92	6.32	5.31
20 story						
50% cut	9.00	9.04	7.02	9.01	9.04	7.03
40% cut	6.59	6.62	5.14	6.59	6.62	5.14

Table 4. Maximum Story Drift Ratio and Roof Displacement Normalized to CTC Model of Frame without RBS

Maximum Story Drift Ratio									
Frame	Without RBS			With 50 % reduction			With 40 % reduction		
Model	CTC	REO	PZ	CTC	REO	PZ	CTC	REO	PZ
3 story	1	0.880	0.981	1.073	0.950	1.042	1.053	0.931	1.026
9 story	1	0.865	0.893	1.067	0.926	0.949	1.049	0.910	0.934
20 story	1	0.858	0.870	1.075	0.923	0.941	1.055	0.906	0.922
Roof Displacement									
Frame	Without RBS			With 50 % reduction			With 40 % reduction		
Model	CTC	REO	PZ	CTC	REO	PZ	CTC	REO	PZ
3 story	1	0.899	1.002	1.071	0.966	1.063	1.052	0.948	1.047
9 story	1	0.868	0.956	1.081	0.943	1.026	1.059	0.923	1.007
20 story	1	0.851	0.916	1.091	0.928	0.980	1.066	0.907	0.963

little difference between the results obtained by the two methods. Therefore, it is suggested that the simplified approach, which uses a prismatic beam element to model beams with the RBS cutouts, can be used as a useful tool to estimate quite exactly the maximum story drift ratios of frames with the RBS cutouts.

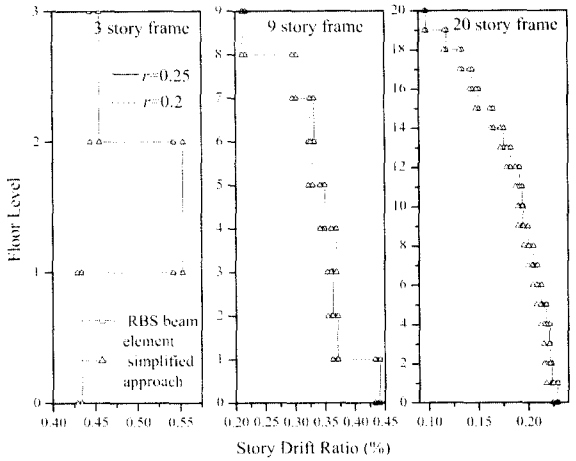

Fig 14. Comparison of Story Drift Ratios Obtained by RBS Beam Element and Simplified Approach

8. Conclusion

This paper presents the formulation for a non-prismatic beam element to model steel beams with reduced beam section (RBS) connection. The element can be used to investigate the effects of the post-Northridge connections on seismic behavior of steel moment frames. It employs the closed-form elastic stiffness matrix including elastic shear effects. A simplified approach is also suggested, which uses a prismatic beam element to model beams with the RBS connection. This method can estimate quite exactly the maximum story drift ratios of frames with the RBS connection with little effort. The effects of reduced beam section connection on the elastic stiffness of steel moment frames were investigated. When 50 percent of the flange width is cutout, the increase in maximum story drift ranges from 6 to 8 percent. For the cutout of 40 percent, the increase in maximum story drift is 4.5 to 6 percent. It should be also noted that the selection of proper model to account for deformations at the joint might have more important role in estimating the maximum story drift ratios of frames correctly than the RBS cutouts.

9. References

ABAQUS. (1996). *User's manual-version 5.6.* Hibbit, Karlsson, and Sorenson, Inc., Pawtucket, R.I.

Chen, S.J., Yeh, C.H. and Chu, J.M. (1996). "Ductile steel beam to column connections for seismic resistance." *J. Struct. Engrg.*, ASCE, 122(11).

Chambers, J.J., Almudhafar, S., and Stenger, F. (2003). "Effect of reduced beam section frame elements on stiffness of moment frames." *J. Struct. Engrg.*, ASCE, 129(3), 383-394.

Engelhardt, M.D., Winneberger, T., Zekany, A.J., and Potyraj, T.J. (1996). "The Dogbone connection: Part II." *Modern Steel Construction*, 36(8), AISC, Chicago, Illinois.

Federal Emergency Management Agency (FEMA) (1995). "Interim Guidelines: evaluation, repair, modification, and design of welded steel moment frame structures." FEMA 267, Washington, D.C.

Federal Emergency Management Agency (FEMA) (2000). "Recommended seismic design criteria for new steel moment-frame buildings." FEMA 350, Washington, D.C.

Faggiano, B., and Landolfo, R. (2003). "Design criteria for RBS in MR frame retrofitting." *Proc., the Conference on Behavior of Steel Structures In Seismic Areas.*, Italy, 683-690.

Grubbs, K.V. (1997). "The effects of the dogbone connection on the elastic stiffness of steel moment frames." Master thesis, Dept. of Civ. Engrg., The University of Texas at Austin, Texas.

Gupta, A. and Krawinkler, H. (1999). "Prediction of seismic demands for SMRFs with ductile connections and elements." *Rep. No. SAC/BD-99/06*, SAC Joint Venture, Sacramento, California.

International Conference of Building Officials (ICBO) (1994). *Uniform building code*, ICBO, Whittier, CA.

Iwankiw, N. (1997). "Ultimate strength consideration for seismic design of the reduced beam section (Internal plastic hinge)." *Engrg. Journal*, First Quarter, AISC, 3-16.

Przemieniecki, J.S. (1968). *Theory of matrix structural*, analysis, McGraw-Hill Book Co., New York, N.Y.

Youssef, N., Bonowitz, D., and Gross, J. (1995). "A survey of steel moment-resisting frame buildings affected by the 1994 Northridge earthquake." *NIST Rep. No. NISTIR 5625, National Institute of Standards and Technology*, United States Dept. of Commerce Technology Administration, Washington, D.C.

(접수일자 : 2004. 9. 6 / 심사일 2004. 9. 23 / 심사완료일 2004. 11. 25)